Solvent-Free Three-Dimensional Printing of Biodegradable Elastomers Using Liquid Macrophotoinitiators

Sandmeier, Matthias; Paunović, Nevena; Conti, Riccardo; Hofmann, Leopold; Wang, Jieping; Luo, Zhi; Masania, Kunal; Wu, Na; Kleger, Nicole; More Authors

Important note
To cite this publication, please use the final published version (if applicable).
Please check the document version above.

Macromolecules

Article

Solvent-Free Three-Dimensional Printing of Biodegradable Elastomers Using Liquid Macrophotoinitiators

Matthias Sandmeier, Nevena Paunović, Riccardo Conti, Leopold Hofmann, Jieping Wang, Zhi Luo, Kunal Masania, Na Wu, Nicole Kleger, Fergal Brian Coulter, André R. Studart, Hansjörg Grützmacher, Jean-Christophe Leroux,* and Yinyin Bao*
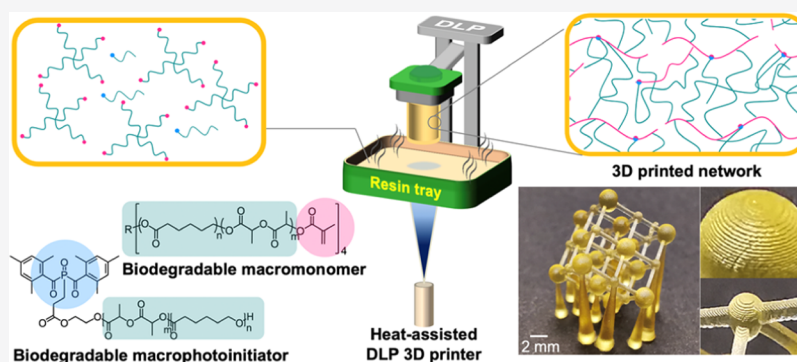
Cite This: *Macromolecules* 2021, 54, 7830−7839

Read Online

ACCESS | Metrics & More | Article Recommendations | Supporting Information

ABSTRACT: Vat photopolymerization 3D printing provides new opportunities for the fabrication of tissue scaffolds and medical devices. However, for the manufacturing of biodegradable elastomers, it usually requires the use of organic solvents to dissolve the solid photoinitiators and achieve low resin viscosity, making this process environmentally unfriendly and not optimal for biomedical applications. Here, we report solvent-free 3D printing of biodegradable elastomers by digital light processing with well-defined photoinitiator−polymer conjugates. Being in liquid state at room temperature, the macrophotoinitiators enabled high-quality 3D printing in the absence of any organic solvents that are usually used in digital light 3D printing. This allowed the systematic investigation of structure−property relationships of 3D-printed biodegradable elastomers without the interference from reactive diluents. The developed macrophotoinitiators were compatible with various photopolymers and could be applied for solvent-free fabrication of biodegradable shape-memory devices. This work offers new perspectives for the solvent-free additive manufacturing of bioresorbable medical implants and other functional devices.

■ INTRODUCTION

Additive manufacturing, or commonly called 3D printing, is attracting great attention due to its powerful ability to create 3D geometries with precise macro- and microarchitectures.[1] In combination with computer-assisted design and medical imaging techniques, it has enormous potential in the biomedical field for applications such as tissue engineering,[2−4] drug delivery,[5−7] soft robotics,[8−10] and the fabrication of medical devices.[11−14] Among the existing 3D printing techniques, vat photopolymerization is endowed with high resolution and good surface quality, which are highly desired in manufacturing of complex objects, such as personalized medical devices.[15,16] With stereolithography (SLA) and digital light processing (DLP) as the best-known examples, vat photopolymerization 3D printing is based on a localized UV radiation-triggered photo-cross-linking process that takes place in a vat containing a liquid resin made of (macro)monomers and a photoinitiator. Through the layer-by-layer cross-linking

of the (macro)monomers, which is typically triggered by the photolysis of the photoinitiator into the primary radicals, the photocurable resin is converted to a solid product.[17,18] Owing to its great advantages, the last 10 years have witnessed the fast development of vat photopolymerization 3D printing in terms of both techniques and materials used.[19−26]

Despite the various benefits of SLA, DLP, and their advanced editions,[27−29] some caveats remain, especially when the manufacturing of bioresorbable medical devices is sought.[30−32] The main drawbacks include the necessity of adding organic solvents such as nonreactive (volatile
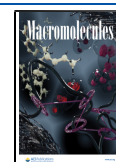
Scheme 1. (a) Synthesis of BAPO-HEA-Poly(DLLA-*co*-CL) (P1) from BAPO-HEA by Random Copolymerization of DLLA and CL (P1); (b) Synthesis of BAPO-DIOL-Poly(DLLA-*co*-CL) (P2) from BAPO-DIOL by Random Copolymerization of DLLA and CL; (c) Chemical 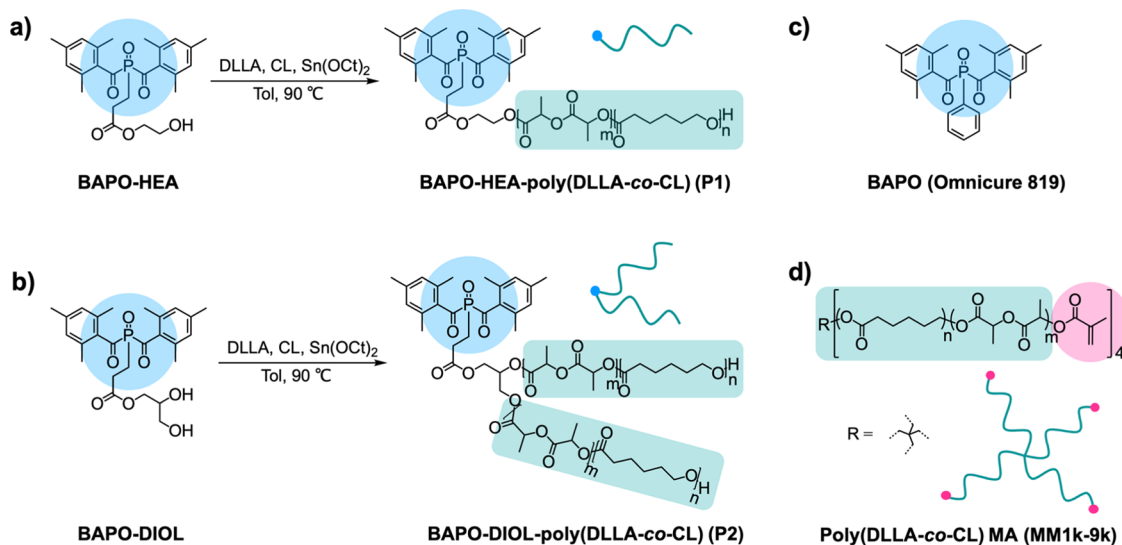Structure of a Commercially Available BAPO (Omnicure 819); (d) Chemical Structure of the Macromonomer Poly(DLLA-*co*-CL) MA (MM1k-9k) Used for 3D Printing

compounds) or reactive diluents (liquid monomers with low viscosity) in the resins formulated with long-chain macromonomers and the use of potentially cytotoxic photoinitiators.[11−13,31−34] Conventional biodegradable 3D printing macromonomers, such as methacrylated poly(lactide) (PLA),[35,36] poly(ε-caprolactone) (PCL),[37−39] and poly-(propylene fumarate),[40−42] are thermoplastic polymers that are in a solid state at ambient temperature due to their high glass transition temperature (T_g) and/or melting point. To achieve low resin viscosity (1−5 mPa·s) required for SLA or DLP, 30−50 wt % of a diluent is usually added to the macromonomers.[35−42] Moreover, both volatile organic solvents and reactive diluents are used to dissolve the photoinitiator molecules in order to homogeneously mix them with the macromonomers. However, removing the volatile organic solvents (*e.g.*, CHCl$_3$) before the printing process carries the risk of undesired premature cross-linking, while postprinting removal causes a shrinkage of the object that can negatively impact its mechanical properties. Furthermore, the addition of reactive diluents can change the structure of the cross-linked network and its cross-linking density, thus potentially reducing the degradability of the 3D printed devices.[31,34−42] On the other hand, the photoinitiators commonly used for 3D printing [*e.g.*, phenylbis(2,4,6-trimethylbenzoyl)phosphine oxide] and their byproducts are usually cytotoxic upon UV irradiation.[43,44] The remaining residues have therefore raised safety concerns.[45,46]

Recently, grafting photoinitiating groups onto polymer chains has become an effective way to decrease the amount of potentially toxic products in the photopolymerization systems and to improve the compatibility of the photoinitiators with the macromonomers in the resins.[45−48] However, there are only a few macrophotoinitiators exploited for 3D printing by vat photopolymerization, and they are only used to prepare hydrogels or solvent-rich resins.[49−51] This is likely due to the fact that the current polymeric photoinitiators are all in a solid state and hardly miscible with 3D printing macromonomers in the absence of organic solvents. Therefore, they are unsuitable for the preparation of a solvent-free resin and further 3D

printing of biodegradable elastomers. We hypothesized that a macrophotoinitiator that is liquid under ambient conditions would allow solvent-free photopolymerization 3D printing by simply mixing the photoinitiator with suitable macromonomers. Here, we present a versatile strategy using well-defined macrophotoinitiators for solvent-free 3D printing of biodegradable polymeric materials. By covalently linking the photoinitiator to a biodegradable polymer chain with structural similarity to the macromonomers, the preparation and 3D printing of the photocurable resin could be both conducted without the addition of any organic solvent or reactive diluent. This may greatly expand the space to enhance the mechanical performance of 3D printed biodegradable elastomers.

■ RESULTS AND DISCUSSION

Monoacylphosphane oxide (MAPO)- and bisacylphosphane oxide (BAPO)-based photoinitiators are widely used in photopolymerization due to their ability to generate free radicals under light irradiation.[52] Among these photoinitiators, phenylbis(2,4,6-trimethylbenzoyl)phosphine oxide (Omnicure 819, formerly known as Irgacure 819) has become one of the most commonly used ones in SLA and DLP, owing to its high absorption in the visible-light region, as well as the prominent use of safe and low-cost 405 nm LED in 3D printers.[31,34,52,53] To enable the preparation of efficient macrophotoinitiators, two BAPO derivatives functionalized with 2-hydroxyethyl acrylate (HEA) or 2,3-dihydroxypropyl acrylate (DIOL-A) were synthesized according to reported methods.[50,52] Hereafter, these are named BAPO-HEA and BAPO-DIOL, respectively, and their structural formulas are shown in Scheme 1. These two compounds were subsequently used as the initiators for ring-opening polymerization of a mixture of D,L-lactide (DLLA) and ε-caprolactone (CL), which led to two well-defined polymers bearing BAPO at the chain end or at the midpoint (Supporting Information, Figures S1−S6). As shown in Table 1, the resulting polymers, BAPO-HEA-poly(DLLA-*co*-CL) (P1) and BAPO-DIOL-poly(DLLA-*co*-CL) (P2), had molecular weights (MWs) of 1990 and 2360 g mol^{-1} by ^{1}H NMR, respectively (see Table 1 and Supporting Information).

Table 1. Characterization of BAPO Polymers

| BAPO polymer	$M_{n,NMR}$[a] (g mol^{-1})	DP_{LA}[a]	DP_{CL}[a]	T_g[b] (°C)	λ_{abs}[c] (nm)	BAPO content[d] (wt %)
P1	1990	3.5	9	−33.7	371, 402	23.0
P2	2360	5.5	9.5	−26.5	371, 401	20.7

[a]Degree of polymerization (DP) calculated from the ratio of the areas under the peak of DLLA (proton −CH−), CL (proton −COOCH$_2$−), and BAPO (aromatic protons). $M_{n,NMR}$ = MW_{BAPO} + MW_{LA} × DP_{LA} + MW_{CL} × DP_{CL}. [b]Determined by DSC. [c]Determined by spectrophotometry. [d]Calculated from the ratio of MW of BAPO-HEA or BAPO-DIOL and the corresponding polymer $M_{n,NMR}$.

Owing to the amorphous nature of the attached random copolymer chains, both polymers were liquid at room temperature, with glass transition temperatures (T_g) of −33.7 and −26.5 °C, respectively (Figure 1a). This is consistent with previous reports[54,55] and our recent work on random copolymers.[56] The light absorption of the BAPO polymers was measured in tetrahydrofuran (THF) (0.1 mM) and compared to the commercial BAPO photoinitiator. Both BAPO polymers showed strong absorption in the range of 360−450 nm, similar to BAPO (Figure 1b). This is important for the efficient 3D printing of biodegradable macromonomers with relatively long chains, as the amount of cross-linkable groups is much lower compared to conventional acrylate monomer-based resins. Different from their nonpolymeric counterpart, the BAPO polymers had the same level of absorption in the visible-light (>400 nm) and the UV-light region. The molar extinction coefficients of P1 and P2 at 405

nm were 438 and 354 M^{-1}·cm^{-1}, respectively, and they were comparable to that of BAPO (514 M^{-1}·cm^{-1}). Consequently, P1 and P2 should efficiently generate radicals under visible LED light irradiation, initiate radical polymerization reactions, and hence enable DLP 3D printing.

To evaluate the 3D printing ability of the BAPO polymers, we synthesized a series of biodegradable macromonomers with $M_{n,NMR}$ ranging from 1200 to 9100 g mol^{-1} (MM1k−9k) by copolymerizing DLLA and CL, with subsequent methacrylation to introduce the cross-linkable moieties (Scheme 1, Figure S7, and Tables S1 and S2)[56,57] and tested the miscibility of the BAPO polymers with the macromonomers. As shown in Figure 1c, the mixture of P1 and the macromonomers produced a transparent solvent-free photoresin. In contrast, the commercial BAPO photoinitiator remained suspended in the resin, even after 1 h of sonication at 60 °C. Although diphenyl(2,4,6-trimethylbenzoyl)phosphine oxide (TPO) had better miscibility with MM9k (Figure S8), it is less used in the visible-light 3D printing of macromonomers due to the lower absorption at 405 nm.[58]

To determine the characteristic penetration depth of the resins, we measured the curing depth (thickness of polymerized resin) of poly(DLLA-co-CL) MA in the presence of BAPO polymers after different DLP laser exposure times (Figure 1d−f). As shown in Figure 1e, the curing depth of MM9k with 2.3 wt % P1 gradually increased from 50 to 750 μm with the increase of the exposure time from 2 to 20 s. The characteristic penetration depth of P1-MM9k resin was determined to be 385 μm (Figure S9).[14] When the P1 concentration was decreased to 1.0 wt %, the penetration depth was reduced to 157 μm. The curing test was also performed with P2-MM7k, producing results similar to P1 (Figures 1f and S10a). Attenuated total reflectance−Fourier
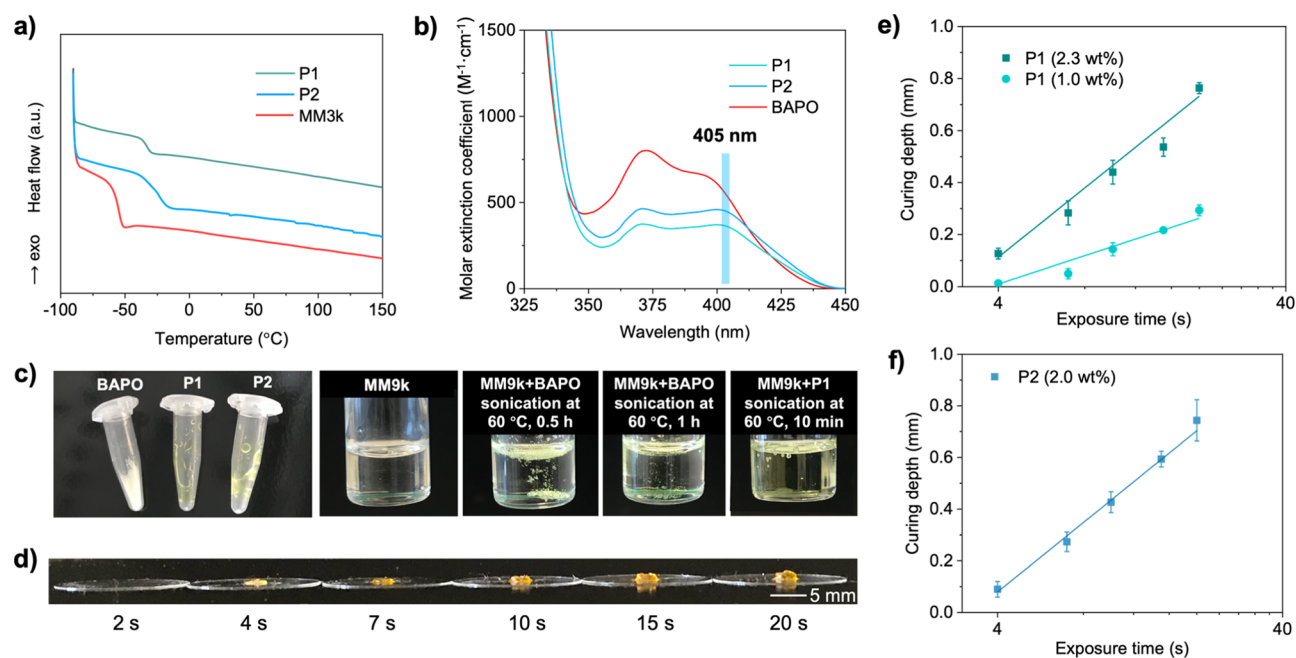
Figure 1. (a) DSC curves of MM3k (3000 g mol^{-1}) and BAPO polymers; (b) absorption spectra of BAPO and BAPO polymers in THF (0.1 mM equiv BAPO); (c) photographs of MM9k, BAPO, and BAPO polymers and the resins containing BAPO (1.0 wt %) or P1 (2.3 wt %); (d) photograph of the cross-linked materials (P1-MM9k with 2.3 wt % P1) after various exposure times (side view). (e) Curing depth−exposure time relationship of the resin with P1-MM9k (2.3 wt % P2). The curing depth is expressed as mean ± s.d. (n = 3). (f) Curing depth−exposure time relationship of the resin with P2-MM7k (2.0 wt % P2). The curing depth is expressed as mean ± s.d. (n = 3). The light intensity was 25.67 mW/cm^2.
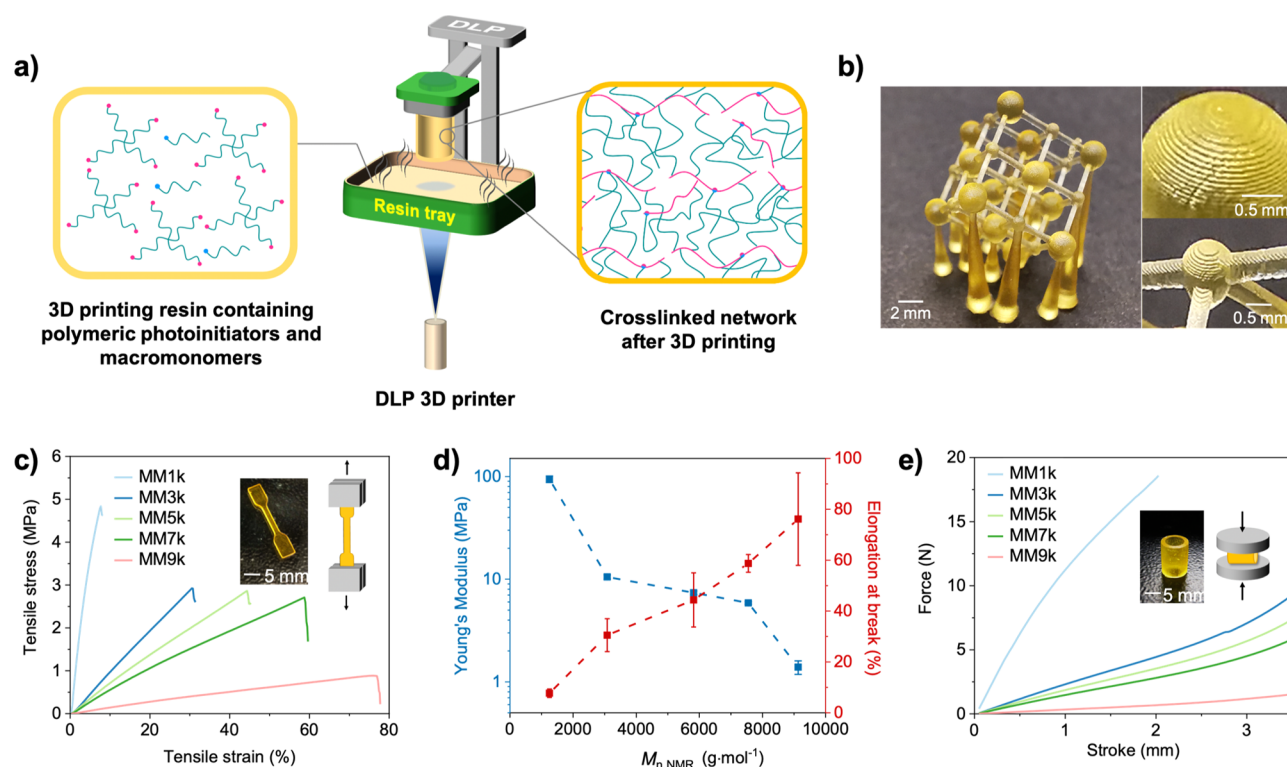
Figure 2. (a) Schematic illustration of 3D printing of biodegradable photopolymers by DLP in the presence of polymeric photoinitiators (the digital micromirror device is not shown for simplification); (b) photograph of a 3D printed model of NaCl crystal with supports and the zoomed area of the balls representing Cl^- and Na^+ while the connecting rods representing the ionic bonds. The layer thickness was calculated to be ~47 μm, which is comparable to the set value of the DLP printer (50 μm); (c) representative stress−strain curves from the tensile test based on 3D printed specimens of poly(DLLA-*co*-CL) MA with various MWs using P1 as the photoinitiator. Inset: Photographs of representative dog-bone-shaped specimens; (d) Young's modulus and maximal elongation as a function of the $M_{n,NMR}$ of the macromonomers. The mechanical properties were obtained from the tensile tests and are expressed as mean ± s.d. ($n = 8$); (e) representative force−stroke curves from the compression test based on 3D printed specimens of poly(DLLA-*co*-CL) MA with various MWs using P1 as the photoinitiator. Inset: Photographs of representative tubular specimens.
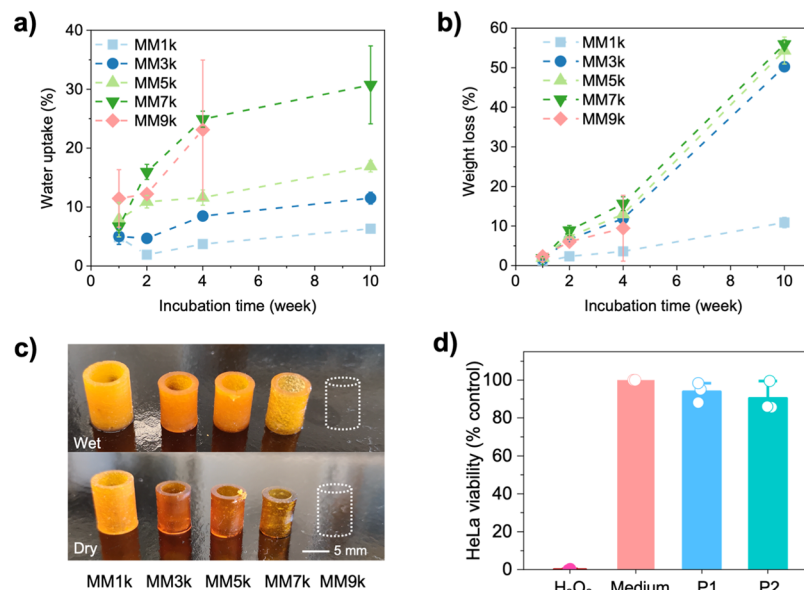
Figure 3. (a−c) Degradation study of 3D printed tubular specimens from poly(DLLA-*co*-CL) MA with various MWs using P1 as the photoinitiator (50 °C in PBS pH 7.4). (a) Water uptake over the incubation time; (b) weight loss depending on the incubation time. All data are expressed as mean ± s.d. ($n = 4$); (c) Photographs of the tubular specimens from P1-MM1k−9k after 10 weeks of incubation. The P1-MM9k specimens collapsed at week 8; (d) HeLa cell viability after 48 h incubation (37 °C) with P1-MM9k (blue) and P2-MM7k (green) 3D printed discs determined by the MTS assay relative to the negative control (cell culture medium, pink). Positive control (100 mM H_2O_2) is presented with a magenta bar. Mean + s.d. ($n = 3$).
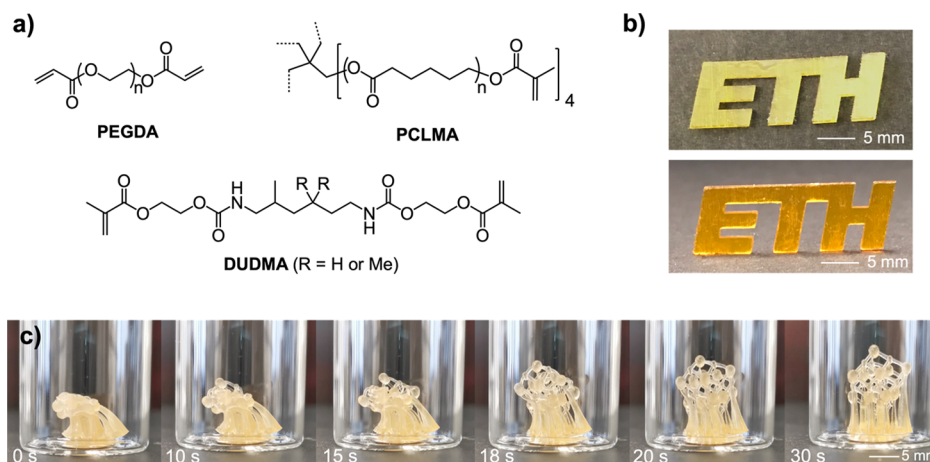
Figure 4. (a) Chemical structures of PEGDA, DUDMA, and PCLMA; (b) 3D-printed ETH logo with PEGDA and DUDMA, respectively, using P1 as the photoinitiator; (c) NaCl crystal model printed by DLP with P1-PCLMA reverting to its original shape upon heating to ∼80 °C. The initial object (at 0 s) was deformed at ∼80 °C and fixed in that shape by cooling to −20 °C.

transform infrared (ATR−FTIR) spectroscopy analysis of P1-MM1k−9k resins before and after 3D printing revealed the high conversion of double bonds of the macromonomers for all compositions, as shown by the disappearance of the vinyl peak at ∼1640 cm^{-1} (Figure S11). This confirms that the light absorption capability of the macrophotoinitiators is sufficient to initiate the polymerization process for 3D printing.

Heat-assisted digital light 3D printing has been employed in the fabrication of objects with complex architectures from highly viscous photopolymer resins that are not printable using conventional SLA or DLP.[39,55,56] We therefore used a customized DLP 3D printer equipped with a heating system and evaluated the performance of the polymeric photo-initiators by printing without any diluent, a NaCl crystal model with P1-MM7k at 80−90 °C (Figure 2a). The 3D printed crystal lattice showed high resolution and a smooth surface (Figure 2b), which was also demonstrated by 3D printed objects with microfeatures (Figure S14). Notably, the equivalent BAPO concentration in the 3D printing resin was only *ca.* 0.5 wt %, which is lower than the usual content of conventional photoinitiators (1.0−4.0 wt %).[30−42] The photoinitiator P2 enabled equally high-quality DLP 3D printing (Figure S10b). The tensile test revealed that the mechanical properties of the printed materials were highly dependent on the polymer chain length (Figure 2c,d). When $M_{n,NMR}$ increased from 1200 to 9100 g mol^{-1}, Young's modulus (Figure 2d) decreased from 94 to 1.0 MPa and the tensile strength (Figure 2c) decreased from 5.0 to 1.0 MPa. This was accompanied by an increase in strain at break from 10 to 80% (Figure 2d). Molecular weight-dependent compressive resistance was also observed in the test on 3D printed stent-mimicking tubular specimens (Figure 2e). The ones prepared with MM1k showed the highest rigidity, while the highest flexibility was obtained with the MM9k resin. These results indicate that our polymeric photoinitiators offer an attractive platform to control the properties of the printed polymers and to systematically investigate their structure−property relationships without the interference of the reactive diluents commonly used in SLA or DLP 3D printing of biodegradable polymers.[31,34]

To further study the influence of MW on the degradation profile of the 3D printed macromonomers, we monitored the water uptake, weight loss, and change in compressive resistance of the tubular specimens incubated in PBS (pH 7.4) at 50 °C over time. As shown in Figure 3a, the water uptake of the specimens increased with time, reflecting the increase in hydrophilicity of the polymer matrix occurring upon degradation. Polymers with longer chains were associated with higher water uptake due to the lower cross-linking density and thus higher water permeability.[59] Consequently, the tubular objects prepared with higher MW macromonomers degraded faster (*e.g.*, P1-MM7k showed ∼55% of weight loss *vs* ∼10% for P1-MM1k after 10 weeks), with the P1-MM9k specimen collapsing already at week 8 (Figure 3b,c). The degradation was accelerated at the later stage, probably due to the increase in hydrophilicity of the network with newly formed carboxyl and hydroxyl groups. As expected, all 3D printed tubular specimens exhibited a continuous decrease in compressive resistance during the degradation process (Figure S12).

To assess cytocompatibility, the 3D printed discs from P1-MM9k and P2-MM7k were incubated with HeLa cells on the top of Transwell inserts[60] and cell viability was determined by the 3-(4,5-dimethylthiazol-2-yl)-5-(3-carboxymethoxyphenyl)-2-(4-sulfophenyl)-2H-tetrazolium (MTS) assay after 48 h of incubation. As shown in Figure 3d, the printed disks did not exhibit significant *in vitro* cytotoxicity under the tested conditions. We expect that the toxicity risk stemming from residual initiators and photolysis products in 3D printed implants *in vivo* can be reduced by employing polymer-conjugated photoinitiating moieties due to their limited migration in the polymeric matrix and slower release rate. In addition, we performed accelerated degradation of the 3D printed products in PBS at 50 °C for 4 days and collected the degradation products after lyophilization. After dissolution and further dilution 1:1 v/v in cell culture medium, their cytotoxicity was tested. As shown in Figure S15, the cells remained *ca.* 100% viable after 24 h of incubation.

To further illustrate the wide applicability of BAPO macrophotoinitiators, we carried out DLP printing with two different commercial monomers, namely, poly(ethylene glycol) diacrylate (PEGDA, hydrophilic) and diurethane dimethacry-late (DUDMA, mixture of isomers, hydrophobic), that are commonly used in photopolymerization 3D printing (Figure 4a). As shown in Figure 4b, high-quality 3D printing was achieved with both inks, using P1 as the photoinitiator. In

addition, we also fabricated a biodegradable shape memory object using P1 and PCL methacrylate (PCLMA, 8300 g mol^{-1}, Figures 4a and S13),[39,61,62] which is a thermoplastic photopolymer with the melting point around 50 °C. A complex object with programmable and recoverable shapes was printed using the NaCl crystal as a model geometry. The as-printed object was deformed upon heating (∼80 °C) and fixed to a temporary shape after cooling to −20 °C. The shape recovery was then triggered by placing the deformed model in a glass vial that was heated up with a heating gun. As shown in Figure 4, the deformed structure fully recovered its original shape within 30 s.

Since the invention of SLA in 1980s, a significant progress on the photopolymerization 3D printing techniques has been achieved. In 2015, DeSimone et al. invented the continuous liquid interface production (CLIP), an upgraded version of DLP, using an oxygen-permeable polymer film at the bottom of resin tray, which allowed much higher printing speeds compared to conventional DLP.[27] In 2019, both Taylor et al. and Mose et al. independently developed a volumetric additive manufacturing method via tomographic reconstruction, which relies on rotating a photopolymer in a dynamically evolving light field, completely circumventing the traditional vertical layer-by-layer stacking process.[28,29] Recently, a linear volumetric 3D printing named xolography was reported by Hecht and co-workers.[63] It is based on intersecting light beams of different wavelengths in the presence of a photoswitchable photoinitiator, which further pushes the boundaries of resolution and speed of digital light 3D printing. Nevertheless, the development of biocompatible and biodegradable materials suitable for biomedical devices is far behind.

The progress is mainly limited by the imbalance between the low viscosity of the resin required for high-resolution 3D printing and the desired performance of the printed products such as biodegradability and mechanical properties. To tackle this issue, we have recently developed functionalized amorphous copolyesters from DLLA and CL that can be DLP-printed at elevated temperature,[56] resulting in biodegradable elastomers with silicone-like elasticity. Still, 8−15 wt % of N-vinylpyrrolidone (NVP) was needed to dissolve the photoinitiator during the resin preparation. When present in high amounts in the polymer network, the contribution of a polar reactive diluent, such as NVP, on the mechanical properties and degradability of the printed products cannot be neglected.

Although ethyl(2,4,6-trimethylbenzoyl)phenylphosphinate (TPO-L), as a liquid MAPO photoinitiator, shows good miscibility in 3D printing resins, its absorption in the visible-light region (e.g., 405 nm) is 3−4 times lower compared to BAPO,[64] making it nonoptimal for the 3D printing of macromonomers with a low number of photopolymerizable groups. Therefore, the conversion of solid BAPO molecules into liquid macrophotoinitiators would not only eliminate the need of diluents in the ink and improve the photoinitiator−macromonomer compatibility but would also maintain the efficient photopolymerization necessary for high-quality 3D printing. Notably, as a general strategy, the design of the macrophotoinitiators can be easily adapted by selecting different combinations of the monomers and used for the digital light 3D printing of various types of biomaterials. In addition, this strategy could be expanded to other types of photoinitiators, such as the newly developed dyes for green light or even far-red light 3D printing,[65] which are of great

value for biomedical applications. On the other hand, the volumetric printing has enabled the additive manufacturing of highly viscous resins without the need for supporting structures. With this technique, the combination of biodegradable macromonomers and liquid macrophotoinitiators may trigger numerous opportunities for the development of innovative printable biomaterials.

CONCLUSIONS

In summary, we developed BAPO-derived biodegradable macrophotoinitiators for vat photopolymerization 3D printing. Because of their liquid form at room temperature, these initiators are easily miscible with 3D printing macromonomers and can be used for digital light 3D printing of biodegradable devices without the addition of organic solvents or diluents. High resolution and surface quality were achieved for all the printed objects. By ring-opening copolymerization of different monomers from BAPO molecules, various biodegradable polymeric photoinitiators could, in the future, be synthesized and combined with different biodegradable polymer systems for solvent-free 3D printing by SLA, DLP, CLIP, volumetric printing, and beyond. This work opens new perspectives for the solvent-free 3D printing of functional devices, especially for functional bioresorbable implants and scaffolds.

MATERIALS AND METHODS

Materials. Unless stated otherwise, all reagents were used as received without further purification. Pentaerythritol, methacryloyl chloride, triethylamine, THF (extra dry), and acetone (extra dry) were purchased from Acros Organics. CL and diphenyl(2,4,6-trimethylbenzoyl)phosphine oxide (TPO) were obtained from Tokyo Chemical Industry. 3,6-Dimethyl-1,4-dioxane-2,5-dione (D,L-lactide, DLLA) was purchased from Huizhou Foryou Medical Devices Co., Ltd. or Acros Organics. Tin(II)-2-ethylhexanoate (Sn(Oct)$_2$), 2,2-diethyl-1,3-propanediol, sodium bicarbonate (NaHCO$_3$), sodium chloride (NaCl), (+)-α-tocopherol (vitamin E), phenylbis(2,4,6-trimethyl-benzoyl)phosphine oxide (BAPO), 1-(phenyldiazenyl)-naphthalen-2-ol (Sudan I), poly(ethylene glycol) diacrylate, average M_n 700 (PEGDA), diurethane dimethacrylate, a mixture of isomers (DUDMA), and lithium bromide (LiBr) were purchased from Sigma-Aldrich. Hexane, dichloromethane (DCM), and dimethylformamide (DMF) were purchased from Fisher Scientific. Dimethyl sulfoxide-d_6 (DMSO-d_6) was obtained from ReseaChem. Methanol and 2-propanol were provided by VWR Chemicals. PBS was obtained from Thermo Fisher Scientific. BAPO-HEA and BAPO-DIOL were synthesized according to the reported methods.[49,52]

Polymer Synthesis. Poly(DLLA-co-CL) MA (MM1k-9k) were synthesized by ring-opening polymerization of DLLA and CL initiated by pentaerythritol (4-arm structure) with Sn(Oct)$_2$ as a catalyst and postfunctionalization with methacryloyl chloride, according to the reported method.[56] The molecular weight of the polymers was controlled by varying the molar feed ratio of the monomers and initiators ([M]/[I]).

BAPO polymers were synthesized by ring-opening polymerization of DLLA and CL initiated by BAPO-HEA or BAPO-DIOL with Sn(Oct)$_2$ as a catalyst. The molecular weight of the polymers was controlled by varying the molar feed ratio of the monomers and initiators ([M]/[I]).

Synthesis of P1. BAPO-HEA (0.5 g, 1.09 mmol), CL (1.24 g, 10.9 mmol), and DLLA (1.57 g, 10.9 mmol) were added to a Schlenk flask. The flask was exposed to vacuum for 1 h and purged with argon for three cycles to remove water and oxygen. Sn(Oct)$_2$ (3.3 μL, 0.01 mmol) was dissolved in toluene (3 mL) in another flask and purged with argon for 15 min. The solution was injected into the monomer mixture under an argon atmosphere, and the Schlenk flask was then placed in an oil bath at 90 °C for 72 h under stirring. The product was

dissolved in THF and precipitated in hexane, resulting in a light-yellow and highly viscous polymer P1.

Synthesis of P2. BAPO-DIOL (0.24 g, 0.5 mmol), CL (0.4 g, 3.5 mmol), and DLLA (0.22 g, 1.5 mmol) were added to a Schlenk flask. The flask was exposed to vacuum for 1 h and purged with argon for three cycles to remove water and oxygen. $Sn(Oct)_2$ (2.0 μL, 0.006 mmol) was dissolved in toluene (1.8 mL) in another flask and purged with argon for 15 min. The solution was injected to the monomer mixtures under an argon atmosphere, and the Schlenk flask was then placed in an oil bath at 80 °C for 24 h under stirring. The product was dissolved in THF and precipitated in hexane, resulting in a light-yellow and highly viscous polymer P2.

Polymer Characterization. ^{1}H NMR spectra were recorded on a Bruker AV400 spectrometer at 400 Hz using DMSO-d_6 as a solvent. Size-exclusion chromatography (SEC) was carried out on a Viscotek TDAmax system equipped with two Viscotek columns (D3000, poly(styrene-*co*-divinylbenzene)) and a differential refractive index detector (TDA 302, Viscotek). All samples were dissolved in DMF, filtered using 0.2 μm syringe filters (polytetrafluoroethylene, PTFE), and eluted using DMF with LiBr (0.1 wt %) as the mobile phase (mobile phase flow: 0.5 mL min⁻¹). The macromolecular characteristics were determined relative to a poly(methyl methacrylate) (PMMA) standard curve (PSS polymer Mainz, 2500−89,300 g mol⁻¹). Differential scanning calorimetry (DSC) analysis was performed using TA Q200 DSC (TA Instruments−Waters LLC). The samples (*ca.* 10 mg) were placed on Tzero hermetic pans (TA Instruments−Waters LLC) and exposed to heat−cool−heat cycles from −80 to 200 °C under nitrogen flow (50 mL min⁻¹) using a heating and cooling rate of 10 °C min⁻¹. Data were analyzed using TA Instruments Universal Analysis 2000 software (5.5.3). The FTIR spectra were recorded on a PerkinElmer Spectrum 65 (PerkinElmer Corporation) in the transmission mode in the range of 600 to 4000 cm⁻¹. The mass spectra were measured on a MALDI-TOF/TOF mass spectrometer (model 5800, AB Sciex, Darmstadt, Germany) equipped with a Nd:YAG laser (355 nm). Polymers were prepared in DCM at a concentration of 100 μM, with an addition of 1 mg/mL NaI as an activating agent. All samples were then mixed with a 40 mg/mL solution of cyano-hydroxy cinnamic acid (CHCA) in methanol, 1:1, v/v. Then, 0.5 μL of each sample was spotted on the MALDI steel target plate and dried in the air before the analysis. All measurements were performed in the reflection positive mode with standard settings.

DLP 3D Printing. DLP resins were prepared by mixing the macromonomers (MM1k-9k or PCLMA or PEGDA) or DUDMA, BAPO polymeric photoinitiators (1.0−2.3 wt %), Sudan I (0.03 wt %), and vitamin E (0.3 wt %). The resins were sonicated at 60 °C until a homogeneous mixture was obtained. A commercial DLP 3D printer (Asiga PICO2) comprising a LED light source of 405 nm with customized resin tray and printing head with heating functions was used to fabricate all the objects.[56] The printing was performed at a temperature of 90 °C (40 °C for PEGDA and DUDMA), with layer thickness of 50 μm and exposure time of 3−4 s. The light intensity of the printer LED was 25.67 mW/cm². After the printing, the printed objects were cleaned in acetone and 2-propanol and then cured in an Asiga Pico Flash UV chamber for 15 min.

Curing Test. The 3D printing resin was irradiated with a round spot-shaped LED light (405 nm) on the 3D printer with different exposure times ranging from 2 to 20 s, and the thickness of the cross-linked layer was measured using a caliper. The penetration depth (D_p) was calculated according to Jacobs' equation based on the Beer−Lambert law[66] (eq 1)

$$C_d = D_p \ln\left[\frac{E_0}{E_c}\right] \tag{1}$$

where C_d is the depth/thickness of the cured resin, E_0 is the energy of light at the surface, and E_c is the "critical" energy required to initiate polymerization. A semilog plot of C_d versus E_0 produces a straight−line curve with a slope of D_p and an x-intercept of E_c. The exposure time was chosen based on D_p and E_c related to the desired part properties.

Mechanical Test. Tensile and compression tests were performed using an AGS-X (Shimadzu) universal testing machine with a 100 N capacity load cell. Tensile tests were carried out on dog-bone shaped 3D printed specimens (ASTM 638 type IV) with a gauge length of 13 mm at a rate of 20 mm min⁻¹. Every material was tested in sextuplets. Compression tests were performed on tubular 3D printed specimens (H 10.0 mm, Ø 8.0 mm, thickness 1.0 mm) at a rate of 10 mm min⁻¹ with three compressions per sample.[56] Young's modulus E was determined as follows (eq 2)

$$E = \frac{\sigma}{\varepsilon} \tag{2}$$

where σ is the engineering stress and ε is the engineering strain.

***In Vitro* Degradation Study.** Four 3D printed tubular specimens (H 10.0 mm, Ø 8.0 mm, and thickness 1.0 mm) were immersed separately in 50 mL PBS pH 7.4 at 50 °C in glass conical flasks. The buffer was replaced weekly. Each time before the test, the specimens were taken out, rinsed with deionized water, wiped with a paper tissue, and dried under vacuum at 50 °C overnight. The water uptake (wt %) was calculated using eq 3

$$\text{water uptake} = \frac{\text{wt}_{\text{wet}} - \text{wt}_{\text{dry}}}{\text{wt}_{\text{dry}}} \times 100 \tag{3}$$

where wt_{wet} is the mass of a stent in a wet state after the wiping, and wt_{dry} is the mass of a stent in a dry state after drying under vacuum. The dried specimens were tested in a uniaxial compression test.[56]

Cell Culture. Human cervical epithelial cells (HeLa, ATCC) were cultured at 37 °C in a humidified atmosphere with 5% CO_2. The cells were used up to passage number 31 and were tested for mycoplasma contamination (MycoAlertTM Mycoplasma Detection Kit, Lonza) at the 10th and last passage number. HeLa cell line was cultured in complete medium containing DMEM (high glucose, GlutaMax, pyruvate, Thermo Fisher Scientific) supplemented with 10% fetal bovine serum (Thermo Fisher Scientific) and 1% penicillin−streptomycin (Thermo Fisher Scientific).

***In Vitro* Cytocompatibility Test.** The test was performed in triplicates in a 24-well plate with a seeding density of 80,000 HeLa cells per well and repeated three times. As a positive control, the cells were incubated in a complete medium with 100 mM hydrogen peroxide, while the complete medium alone was used as a negative control. Cell viability was determined using the MTS assay (CellTiter 96 Aqueous One Solution Cell Proliferation Assay, G3580; Promega) according to the manufacturer's instructions and was calculated as a percentage of the negative control. 3D printed disks (H 0.8 mm, Ø 5.5 mm) and dog-bone-shaped specimens were used for Transwell and extract tests, respectively. The objects were washed in acetone and then in PBS pH 7.4 (50 mL) for 30 min and overnight, respectively. Afterward, the objects were dried under vacuum at room temperature for 24 h and then cured in an Asiga Pico Flash UV chamber for 20 min. For the Transwell test, the disks were soaked in the medium (10 mL) for 20 min before incubation. Immediately after cell seeding, Transwell permeable supports (ThinCert Cell Culture Inserts 24-well, sterile, translucent, pore size 8 μm; Greiner Bio-One) were placed in corresponding wells and 3D printed disks were placed on top of the inserts and covered with the medium (100 μL). The plate was incubated for 48 ± 1 h.[56] For the extract test, after cleaning, four test strips were immersed in 50 mL of PBS in a closed Falcon tube and incubated while shaking at 50 °C for 4 days. The medium was then frozen, lyophilized, reconstituted in the same volume of the complete medium, and diluted 1:1 v/v with the complete medium, respectively. After 24 h of cell seeding, the medium was replaced with diluted extracts or controls and the cells were incubated for additional 24 ± 1 h.

■ ASSOCIATED CONTENT

ⓈⒾ Supporting Information

The Supporting Information is available free of charge at https://pubs.acs.org/doi/10.1021/acs.macromol.1c00856.

NMR, GPC, MALDI-TOF, DSC, and FTIR spectra, and compression stress−strain curves (PDF)

Shape memory demonstration (MP4)

AUTHOR INFORMATION

Corresponding Authors

Jean-Christophe Leroux − *Institute of Pharmaceutical Sciences, Department of Chemistry and Applied Biosciences, ETH Zurich, 8093 Zurich, Switzerland;* orcid.org/0000-0001-5601-1292; Email: jleroux@ethz.ch

Yinyin Bao − *Institute of Pharmaceutical Sciences, Department of Chemistry and Applied Biosciences, ETH Zurich, 8093 Zurich, Switzerland;* orcid.org/0000-0001-5264-1211; Email: yinyin.bao@pharma.ethz.ch, baoyinyin@mail.ustc.edu.cn

Authors

Matthias Sandmeier − *Institute of Pharmaceutical Sciences, Department of Chemistry and Applied Biosciences, ETH Zurich, 8093 Zurich, Switzerland*

Nevena Paunović − *Institute of Pharmaceutical Sciences, Department of Chemistry and Applied Biosciences, ETH Zurich, 8093 Zurich, Switzerland*

Riccardo Conti − *Laboratory of Inorganic Chemistry, Department of Chemistry and Applied Biosciences, ETH Zurich, 8093 Zurich, Switzerland*

Leopold Hofmann − *Institute of Pharmaceutical Sciences, Department of Chemistry and Applied Biosciences, ETH Zurich, 8093 Zurich, Switzerland*

Jieping Wang − *Laboratory of Inorganic Chemistry, Department of Chemistry and Applied Biosciences, ETH Zurich, 8093 Zurich, Switzerland*

Zhi Luo − *Institute of Pharmaceutical Sciences, Department of Chemistry and Applied Biosciences, ETH Zurich, 8093 Zurich, Switzerland;* orcid.org/0000-0001-5590-4849

Kunal Masania − *Complex Materials, Department of Materials, ETH Zurich, 8093 Zurich, Switzerland;* Present Address: Shaping Matter Lab, Faculty of Aerospace, TU Delft, Netherlands; orcid.org/0000-0001-9498-1505

Na Wu − *Lab of Organic Chemistry, Department of Chemistry and Applied Biosciences, ETH Zurich, 8093 Zurich, Switzerland*

Nicole Kleger − *Complex Materials, Department of Materials, ETH Zurich, 8093 Zurich, Switzerland*

Fergal Brian Coulter − *Complex Materials, Department of Materials, ETH Zurich, 8093 Zurich, Switzerland*

André R. Studart − *Complex Materials, Department of Materials, ETH Zurich, 8093 Zurich, Switzerland;* orcid.org/0000-0003-4205-8545

Hansjörg Grützmacher − *Laboratory of Inorganic Chemistry, Department of Chemistry and Applied Biosciences, ETH Zurich, 8093 Zurich, Switzerland*

Complete contact information is available at:
https://pubs.acs.org/10.1021/acs.macromol.1c00856

Author Contributions

M.S. and N.P. contributed equally. The manuscript was written through contributions of all authors. All authors have given approval to the final version of the manuscript.

Notes

The authors declare no competing financial interest.

REFERENCES

(1) Guvendiren, M.; Molde, J.; Soares, R. M. D.; Kohn, J. Designing Biomaterials for 3D Printing. *ACS Biomater. Sci. Eng.* **2016**, *2*, 1679−1693.

(2) Do, A.-V.; Khorsand, B.; Geary, S. M.; Salem, A. K. 3D Printing of Scaffolds for Tissue Regeneration Applications. *Adv. Healthcare Mater.* **2015**, *4*, 1742−1762.

(3) Ragelle, H.; Tibbitt, M. W.; Wu, S.-Y.; Castillo, M. A.; Cheng, G. Z.; Gangadharan, S. P.; Anderson, D. G.; Cima, M. J.; Langer, R. Surface Tension-Assisted Additive Manufacturing. *Nat. Commun.* **2018**, *9*, 1184.

(4) Mondschein, R. J.; Kanitkar, A.; Williams, C. B.; Verbridge, S. S.; Long, T. E. Polymer Structure-Property Requirements for Stereolithographic 3D Printing of Soft Tissue Engineering Scaffolds. *Biomaterials* **2017**, *140*, 170−188.

(5) Goole, J.; Amighi, K. 3D Printing in Pharmaceutics: A New Tool for Designing Customized Drug Delivery Systems. *Int. J. Pharm.* **2016**, *499*, 376−394.

(6) Liang, K.; Carmone, S.; Brambilla, D.; Leroux, J.-C. 3D Printing of a Wearable Personalized Oral Delivery Device: A First-in-Human Study. *Sci. Adv.* **2018**, *4*, No. eaat2544.

(7) Oh, H. J.; Aboian, M. S.; Yi, M. Y. J.; Maslyn, J. A.; Loo, W. S.; Jiang, X.; Parkinson, D. Y.; Wilson, M. W.; Moore, T.; Yee, C. R.; Robbins, G. R.; Barth, F. M.; Desimone, J. M.; Hetts, S. W.; Balsara, N. P. 3D Printed Absorber for Capturing Chemotherapy Drugs before They Spread through the Body. *ACS Cent. Sci.* **2019**, *5*, 419−427.

(8) Wallin, T. J.; Pikul, J.; Shepherd, R. F. 3D Printing of Soft Robotic Systems. *Nat. Rev. Mater.* **2018**, *3*, 84−100.

(9) Huang, T.-Y.; Sakar, M. S.; Mao, A.; Petruska, A. J.; Qiu, F.; Chen, X.-B.; Kennedy, S.; Mooney, D.; Nelson, B. J. 3D Printed Microtransporters: Compound Micromachines for Spatiotemporally Controlled Delivery of Therapeutic Agents. *Adv. Mater.* **2015**, *27*, 6644−6650.

(10) Sachyani Keneth, E.; Kamyshny, A.; Totaro, M.; Beccai, L.; Magdassi, S. 3D Printing Materials for Soft Robotics. *Adv. Mater.* **2020**, *33*, 2003387.

(11) Nagarajan, N.; Dupret-Bories, A.; Karabulut, E.; Zorlutuna, P.; Vrana, N. E. Enabling Personalized Implant and Controllable Biosystem Development through 3D Printing. *Biotechnol. Adv.* **2018**, *36*, 521−533.

(12) Hwang, H. H.; Zhu, W.; Victorine, G.; Lawrence, N.; Chen, S. 3D-Printing of Functional Biomedical Microdevices via Light- and Extrusion-Based Approaches. *Small Methods* **2018**, *2*, 1700277.

(13) Lind, J. U.; Busbee, T. A.; Valentine, A. D.; Pasqualini, F. S.; Yuan, H.; Yadid, M.; Park, S.-J.; Kotikian, A.; Nesmith, A. P.; Campbell, P. H.; Vlassak, J. J.; Lewis, J. A.; Parker, K. K. Instrumented Cardiac Microphysiological Devices via Multimaterial Three-Dimensional Printing. *Nat. Mater.* **2017**, *16*, 303−308.

(14) Bhattacharjee, N.; Parra-Cabrera, C.; Kim, Y. T.; Kuo, A. P.; Folch, A. Desktop-Stereolithography 3D-Printing of a Poly-(Dimethylsiloxane)-Based Material with Sylgard-184 Properties. *Adv. Mater.* **2018**, *30*, 1800001.

(15) Chartrain, N. A.; Williams, C. B.; Whittington, A. R. A Review on Fabricating Tissue Scaffolds Using Vat Photopolymerization. *Acta Biomater.* **2018**, *74*, 90−111.

(16) Melchels, F. P. W.; Feijen, J.; Grijpma, D. W. A Review on Stereolithography and Its Applications in Biomedical Engineering. *Biomaterials* **2010**, *31*, 6121−6130.

(17) Bagheri, A.; Jin, J. Photopolymerization in 3D Printing. *ACS Appl. Polym. Mater.* **2019**, *1*, 593−611.

(18) Yu, C.; Schimelman, J.; Wang, P.; Miller, K. L.; Ma, X.; You, S.; Guan, J.; Sun, B.; Zhu, W.; Chen, S. Photopolymerizable Biomaterials and Light-Based 3D Printing Strategies for Biomedical Applications. *Chem. Rev.* **2020**, *120*, 10695−10743.

(19) Layani, M.; Wang, X.; Magdassi, S. Novel Materials for 3D Printing by Photopolymerization. *Adv. Mater.* **2018**, *30*, 1706344.

(20) Seidler, K.; Griesser, M.; Kury, M.; Harikrishna, R.; Dorfinger, P.; Koch, T.; Svirkova, A.; Marchetti-Deschmann, M.; Stampfl, J.; Moszner, N.; Gorsche, C.; Liska, R. Vinyl Sulfonate Esters: Efficient Chain Transfer Agents for the 3D Printing of Tough Photopolymers without Retardation. *Angew. Chem., Int. Ed.* **2018**, *57*, 9165−9169.

(21) Zhang, Z.; Corrigan, N.; Bagheri, A.; Jin, J.; Boyer, C. A Versatile 3D and 4D Printing System through Photocontrolled RAFT Polymerization. *Angew. Chem., Int. Ed.* **2019**, *58*, 17954−17963.

(22) Schwartz, J. J.; Boydston, A. J. Multimaterial Actinic Spatial Control 3D and 4D Printing. *Nat. Commun.* **2019**, *10*, 791.

(23) Zhang, B.; Kowsari, K.; Serjouei, A.; Dunn, M. L.; Ge, Q. Reprocessable Thermosets for Sustainable Three-Dimensional Printing. *Nat. Commun.* **2018**, *9*, 1831.

(24) Dolinski, N. D.; Page, Z. A.; Callaway, E. B.; Eisenreich, F.; Garcia, R. V.; Chavez, R.; Bothman, D. P.; Hecht, S.; Zok, F. W.; Hawker, C. J. Solution Mask Liquid Lithography (SMaLL) for One-Step, Multimaterial 3D Printing. *Adv. Mater.* **2018**, *30*, 1800364.

(25) Kuang, X.; Wu, J.; Chen, K.; Zhao, Z.; Ding, Z.; Hu, F.; Fang, D.; Qi, H. J. Grayscale Digital Light Processing 3D Printing for Highly Functionally Graded Materials. *Sci. Adv.* **2019**, *5*, No. eaav5790.

(26) Moore, D. G.; Barbera, L.; Masania, K.; Studart, A. R. Three-Dimensional Printing of Multicomponent Glasses Using Phase-Separating Resins. *Nat. Mater.* **2020**, *19*, 212−217.

(27) Tumbleston, J. R.; Shirvanyants, D.; Ermoshkin, N.; Janusziewicz, R.; Johnson, A. R.; Kelly, D.; Chen, K.; Pinschmidt, R.; Rolland, J. P.; Ermoshkin, A.; Samulski, E. T.; DeSimone, J. M. Continuous Liquid Interface Production of 3D Objects. *Science* **2015**, *347*, 1349−1352.

(28) Kelly, B. E.; Bhattacharya, I.; Heidari, H.; Shusteff, M.; Spadaccini, C. M.; Taylor, H. K. Volumetric Additive Manufacturing via Tomographic Reconstruction. *Science* **2019**, *363*, 1075−1079.

(29) Loterie, D.; Delrot, P.; Moser, C. High-Resolution Tomographic Volumetric Additive Manufacturing. *Nat. Commun.* **2020**, *11*, 852.

(30) Jose, R. R.; Rodriguez, M. J.; Dixon, T. A.; Omenetto, F.; Kaplan, D. L. Evolution of Bioinks and Additive Manufacturing Technologies for 3D Bioprinting. *ACS Biomater. Sci. Eng.* **2016**, *2*, 1662−1678.

(31) Zhang, J.; Xiao, P. 3D Printing of Photopolymers. *Polym. Chem.* **2018**, *9*, 1530−1540.

(32) Guzzi, E. A.; Tibbitt, M. W. Additive Manufacturing of Precision Biomaterials. *Adv. Mater.* **2020**, *32*, 1901994.

(33) Lim, K. S.; Galarraga, J. H.; Cui, X.; Lindberg, G. C. J.; Burdick, J. A.; Woodfield, T. B. F. Fundamentals and Applications of Photo-Cross-Linking in Bioprinting. *Chem. Rev.* **2020**, *120*, 10662−10694.

(34) Ligon, S. C.; Liska, R.; Stampfl, J.; Gurr, M.; Mülhaupt, R. Polymers for 3D Printing and Customized Additive Manufacturing. *Chem. Rev.* **2017**, *117*, 10212−10290.

(35) Melchels, F. P. W.; Feijen, J.; Grijpma, D. W. A Poly(d,l-Lactide) Resin for the Preparation of Tissue Engineering Scaffolds by Stereolithography. *Biomaterials* **2009**, *30*, 3801−3809.

(36) Seck, T. M.; Melchels, F. P. W.; Feijen, J.; Grijpma, D. W. Designed Biodegradable Hydrogel Structures Prepared by Stereolithography Using Poly(Ethylene Glycol)/Poly(d,l-Lactide)-Based Resins. *J. Controlled Release* **2010**, *148*, 34−41.

(37) Elomaa, L.; Teixeira, S.; Hakala, R.; Korhonen, H.; Grijpma, D. W.; Seppälä, J. V. Preparation of Poly(ε-Caprolactone)-Based Tissue Engineering Scaffolds by Stereolithography. *Acta Biomater.* **2011**, *7*, 3850−3856.

(38) Green, B. J.; Worthington, K. S.; Thompson, J. R.; Bunn, S. J.; Rethwisch, M.; Kaalberg, E. E.; Jiao, C.; Wiley, L. A.; Mullins, R. F.; Stone, E. M.; Sohn, E. H.; Tucker, B. A.; Guymon, C. A. Effect of Molecular Weight and Functionality on Acrylated Poly-(Caprolactone) for Stereolithography and Biomedical Applications. *Biomacromolecules* **2018**, *19*, 3682−3692.

(39) Zarek, M.; Layani, M.; Cooperstein, I.; Sachyani, E.; Cohn, D.; Magdassi, S. 3D Printing of Shape Memory Polymers for Flexible Electronic Devices. *Adv. Mater.* **2016**, *28*, 4449−4454.

(40) Wilson, J. A.; Luong, D.; Kleinfehn, A. P.; Sallam, S.; Wesdemiotis, C.; Becker, M. L. Magnesium Catalyzed Polymerization of End Functionalized Poly(Propylene Maleate) and Poly(Propylene Fumarate) for 3D Printing of Bioactive Scaffolds. *J. Am. Chem. Soc.* **2018**, *140*, 277−284.

(41) Le Fer, G.; Luo, Y.; Becker, M. L. Poly(Propylene Fumarate) Stars, Using Architecture to Reduce the Viscosity of 3D Printable Resins. *Polym. Chem.* **2019**, *10*, 4655−4664.

(42) Luo, Y.; Le Fer, G.; Dean, D.; Becker, M. L. 3D Printing of Poly(Propylene Fumarate) Oligomers: Evaluation of Resin Viscosity, Printing Characteristics and Mechanical Properties. *Biomacromolecules* **2019**, *20*, 1699−1708.

(43) Popal, M.; Volk, J.; Leyhausen, G.; Geurtsen, W. Cytotoxic and Genotoxic Potential of the Type I Photoinitiators BAPO and TPO on Human Oral Keratinocytes and V79 Fibroblasts. *Dent. Mater.* **2018**, *34*, 1783−1796.

(44) Beil, A.; Steudel, F. A.; Bräuchle, C.; Grützmacher, H.; Möckl, L. Bisacylphosphane Oxides as Photo-Latent Cytotoxic Agents and Potential Photo-Latent Anticancer Drugs. *Sci. Rep.* **2019**, *9*, 6003.

(45) Zhou, J.; Allonas, X.; Ibrahim, A.; Liu, X. Progress in the Development of Polymeric and Multifunctional Photoinitiators. *Prog. Polym. Sci.* **2019**, *99*, 101165.

(46) Han, Y.; Wang, F.; Lim, C. Y.; Chi, H.; Chen, D.; Wang, F.; Jiao, X. High-Performance Nano-Photoinitiators with Improved Safety for 3D Printing. *ACS Appl. Mater. Interfaces* **2017**, *9*, 32418−32423.

(47) Degirmenci, M.; Hizal, G.; Yagci, Y. Synthesis and Characterization of Macrophotoinitiators of Poly(ε-Caprolactone) and Their Use in Block Copolymerization. *Macromolecules* **2002**, *35*, 8265−8270.

(48) Baralle, A.; Garra, P.; Graff, B.; Morlet-Savary, F.; Dietlin, C.; Fouassier, J. P.; Lakhdar, S.; Lalevée, J. Iodinated Polystyrene for Polymeric Charge Transfer Complexes: Toward High-Performance Near-UV and Visible Light Macrophotoinitiators. *Macromolecules* **2019**, *52*, 3448−3453.

(49) Wang, J.; Chiappone, A.; Roppolo, I.; Shao, F.; Fantino, E.; Lorusso, M.; Rentsch, D.; Dietliker, K.; Pirri, C. F.; Grützmacher, H. All-in-One Cellulose Nanocrystals for 3D Printing of Nanocomposite Hydrogels. *Angew. Chem., Int. Ed.* **2018**, *57*, 2353−2356.

(50) Wang, J.; Stanic, S.; Altun, A. A.; Schwentenwein, M.; Dietliker, K.; Jin, L.; Stampfl, J.; Baudis, S.; Liska, R.; Grützmacher, H. A Highly Efficient Waterborne Photoinitiator for Visible-Light-Induced Three-Dimensional Printing of Hydrogels. *Chem. Commun.* **2018**, *54*, 920−923.

(51) Zhang, X.; Keck, S.; Qi, Y.; Baudis, S.; Zhao, Y. Study on Modified Dealkaline Lignin as Visible Light Macromolecular Photoinitiator for 3D Printing. *ACS Sustainable Chem. Eng.* **2020**, *8*, 10959−10970.

(52) Wang, J. *Synthesis and Application of Bis(acyl)phosphane Oxide Photoinitiators*; ETH Zurich, 2017.

(53) Sun, K.; Xu, Y.; Dumur, F.; Morlet-Savary, F.; Chen, H.; Dietlin, C.; Graff, B.; Lalevée, J.; Xiao, P. In Silico Rational Design by Molecular Modeling of New Ketones as Photoinitiators in Three-Component Photoinitiating Systems: Application in 3D Printing. *Polym. Chem.* **2020**, *11*, 2230−2242.

(54) Amsden, B. G.; Tse, M. Y.; Turner, N. D.; Knight, D. K.; Pang, S. C. In Vivo Degradation Behavior of Photo-Cross-Linked Star-Poly(ε-Caprolactone-Co-D,L-Lactide) Elastomers. *Biomacromolecules* **2006**, *7*, 365−372.

(55) Kuhnt, T.; Marroquín García, R.; Camarero-Espinosa, S.; Dias, A.; Ten Cate, A. T.; Van Blitterswijk, C. A.; Moroni, L.; Baker, M. B. Poly(Caprolactone -Co -Trimethylenecarbonate) Urethane Acrylate

Resins for Digital Light Processing of Bioresorbable Tissue Engineering Implants. *Biomater. Sci.* **2019**, *7*, 4984−4989.

(56) Paunović, N.; Bao, Y.; Coulter, F. B.; Masania, K.; Geks, A. K.; Klein, K.; Rafsanjani, A.; Cadalbert, J.; Kronen, P. W.; Kleger, N.; Karol, A.; Luo, Z.; Rüber, F.; Brambilla, D.; von Rechenberg, B.; Franzen, D.; Studart, A. R.; Leroux, J. C. Digital Light 3D Printing of Customized Bioresorbable Airway Stents with Elastomeric Properties. *Sci. Adv.* **2021**, *7*, abe9499.

(57) Amsden, B. G.; Misra, G.; Gu, F.; Younes, H. M. Synthesis and Characterization of a Photo-Cross-Linked Biodegradable Elastomer. *Biomacromolecules* **2004**, *5*, 2479−2486.

(58) Sodré, C. S.; Albuquerque, P. P. A. C.; Isolan, C. P.; Moraes, R. R.; Schneider, L. F. Relative Photon Absorption Determination and the Influence of Photoinitiator System and Water Content on C=C Conversion, Water Sorption/Solubility of Experimental Self-Etch Adhesives. *Int. J. Adhes. Adhes.* **2015**, *63*, 152−157.

(59) Younes, H. M.; Bravo-Grimaldo, E.; Amsden, B. G. Synthesis, Characterization and in Vitro Degradation of a Biodegradable Elastomer. *Biomaterials* **2004**, *25*, 5261−5269.

(60) Wang, M. O.; Etheridge, J. M.; Thompson, J. A.; Vorwald, C. E.; Dean, D.; Fisher, J. P. Evaluation of the in Vitro Cytotoxicity of Cross-Linked Biomaterials. *Biomacromolecules* **2013**, *14*, 1321−1329.

(61) Zhang, Y.; Huang, L.; Song, H.; Ni, C.; Wu, J.; Zhao, Q.; Xie, T. 4D Printing of a Digital Shape Memory Polymer with Tunable High Performance. *ACS Appl. Mater. Interfaces* **2019**, *11*, 32408−32413.

(62) Kuang, X.; Roach, D. J.; Wu, J.; Hamel, C. M.; Ding, Z.; Wang, T.; Dunn, M. L.; Qi, H. J. Advances in 4D Printing: Materials and Applications. *Adv. Funct. Mater.* **2019**, *29*, 1805290.

(63) Regehly, M.; Garmshausen, Y.; Reuter, M.; König, N. F.; Israel, E.; Kelly, D. P.; Chou, C.-Y.; Koch, K.; Asfari, B.; Hecht, S. Xolography for Linear Volumetric 3D Printing. *Nature* **2020**, *588*, 620−624.

(64) Steyrer, B.; Neubauer, P.; Liska, R.; Stampfl, J. Visible Light Photoinitiator for 3D-Printing of Tough Methacrylate Resins. *Materials* **2017**, *10*, 1445.

(65) Stafford, A.; Ahn, D.; Raulerson, E. K.; Chung, K.-Y.; Sun, K.; Cadena, D. M.; Forrister, E. M.; Yost, S. R.; Roberts, S. T.; Page, Z. A. Catalyst Halogenation Enables Rapid and Efficient Polymerizations with Visible to Far-Red Light. *J. Am. Chem. Soc.* **2020**, *142*, 14733−14742.

(66) Jacobs, P. F. *Fundamentals of Stereolithography, Society of Manufacturing Engineers in Cooperation with the Computer and Automated Systems Association of SME*, 1992.